https://doi.org/10.15407/ufm.23.01.059

V.Yu. DANILCHENKO*, Ye.M. DZEVIN, and R.M. DELIDON**

G.V. Kurdyumov Institute for Metal Physics of the N.A.S. of Ukraine,
36 Academician Vernadsky Blvd.,
UA-03142 Kyiv, Ukraine

* danila@imp.kiev.ua, ** dzevin@i.ua

REGULARITIES OF MARTENSITIC TRANSFORMATIONS OF Fe–Ni ALLOYS RAPIDLY QUENCHED FROM MELT

The regularities of formation of the grain structure of metastable iron–nickel alloys formed in conditions of high temperature gradients during the melt hardening (spinning) and its effect on the characteristics of martensitic transformations (MT) in local areas of thin ribbons are reviewed and studied. A comparison of the texture of the austenitic and martensitic phases on different sides of thin ribbons is carried out. The consequences of influence of relaxation processes in hardening of thin ribbons on regularities of formation of the grain structure are investigated. The proposed x-ray method of measuring the amount of martensite allows solving the problem of measuring the amount of martensite in the local areas of textured alloys. As established, the completeness of MT is different for the contact and free sides of the ribbon. The main factors, which determine the heterogeneous distribution of the martensitic phase in the local areas of the ribbon, are analysed. The size effects at MP, residual stresses, and changes in the chemical composition of the austenitic phase on the distribution of the martensitic phase in local sections of the ribbon are analysed. The influence of size effect on the direct γ–α- and reverse α–γ-MT in thin ribbons is studied. The role of ultradispersed component of austenitic grains in the stabilization of austenite of rapidly quenched alloys with cyclic γ–α–γ MT is revealed.

Keywords: martensitic transformations, Fe–Ni alloys, melt spinning, ribbon, grain structure, texture, stresses.

Citation: V.Yu. Danilchenko, Ye.M. Dzevin, and R.M. Delidon, Regularities of Martensitic Transformations of Fe–Ni Alloys Rapidly Quenched from Melt, *Progress in Physics of Metals*, **23**, No. 1: 59–89 (2022)

1. Introduction

One of the actual trends of contemporary materials science is the development of metallic materials with specific properties by means of ultra-rapid quenching of the melt (spinning). Due to cooling at a rate of (10^6–10^8) K/s in such materials a specific structural-and-phase state is formed, macro- and micro-inhomogeneities appear, phase components are crumbled, and the region of mutual solubility of chemical elements is significantly expanded. This specifies the formation of a new set of physical and mechanical and exploitation properties of rapidly quenched alloy (RQA) at issue [1–4]. Thereby, intensive research and development of high-dispersed metallic materials has been carried out for the last 20 years.

The main factor affecting the changes in the properties of rapidly quenched materials is the grain size of the phase components. The metal materials of ultra-dispersed (grain size 100–1000 nm) and nanocrystalline (grain size 20–100 nm) structure obtained by quenching from melt [5–8]. There is impossible to obtain such fine grain by traditional methods of thermal treatment. The rapidly quenched materials can be considered as qualitatively new perspective materials of next generation. There are can be used as constructional, instrumental and functional materials. The alloy has an increased strength, hardness, low heating conductivity, high coefficient of grain-border diffusion, improved magnetic characteristics. The further progress in the field of development of the RQAs connected with purposeful management of their nonequilibrium crystallization and structural-and-phase transformations processes in solid state [9–12].

Additional possibilities to control the structure formation of thin-ribbon materials of ferric metastable alloys arise during the martensitic transformations (MT), which realized in a process of super-fast crystallization of melt or during the next cooling and action of external factors. There is a certain prospect for creation the new materials based on the rapidly quenched Fe–Ni alloys, when there are direct and reverse MT at the cooling and subsequent heating. Controlled MT in thin-ribbon materials can be used to strengthen, provide the shape memory effect, improve magnetic (hysteresis) properties, control the temperature expansion coefficient, and some other characteristics of alloys [13–18]. The formation of nanostructures in such materials can be ensured by refining the austenitic and martensitic phases to nanoscale size due to the reverse transformation.

However, the powerful factor of MT for the formation of a new complex of properties of the metastable alloys can be used only if we study the features of such transformations in thin-ribbon materials obtained in sharply nonequilibrium conditions of super-fast cooling.

This article reviews the works in the G.V. Kurdyumov Institute for Metal Physics of the N.A.S. of Ukraine (IMP NASU) to study the features of MT and formation regularities of structural–phase state in the local areas of thin ribbons of metastable iron–nickel alloys, rapidly quenched from melt.

2. Materials and Methods

The alloys were selected in such way that the processes of formation of fine grains and the formation of martensite took place in stages: first, a rapidly hardened structure of the initial γ-phase was formed, and then at temperatures below room the MT was realized. Ribbons obtained from iron–nickel melts of alloy *1* (31.4 wt.% Ni and 0.03 wt.% C) and alloy *2* (28 wt.% Ni, 2.1 wt.% Ti, 2 wt.% Al, and 0.05 wt.% C) were used as objects of the study. They were obtained in a carbon dioxide atmosphere at a cooling rate 10^5–10^6 K/s. The alloy *1* ribbon was of 30 μm thick and 8 mm wide, and the alloy *2* ribbon was of 18 μm and 5 mm, respectively. Continuous ribbons were obtained by spinning of a 100 g of melt by casting its flat jet on the outer surface of a massive copper disk rotating at a speed of 4000 rpm [19]. At room temperature, the ribbons were in an austenitic state. Direct transformation was realized by cooling in liquid nitrogen, and the reverse one was realized through heating in a salt bath with a temperature 450–500 °C. The ribbons were obtained in the IMP NASU.

Laser processing (LP) was performed at the Quant-18M equipment (pulsed solid-state laser on neodymium glass active elements, radiation wavelength — 1.06 μm, pulse duration — 8 ms, impulse power — 8–20 J/mm^2). The source of energy was controlled by calorimetric measurements of ICT-1H. The surface of the samples was treated with single pulses with a follow-up period of one second with mutual overlap of laser spots by 30–40%. LP was carried out in the mode of laser heating in the γ-region 0.1–0.45 J/mm^2, pre-melting 0.5–0.7 J/mm^2 and melting 0.8–2.0 J/mm^2. In the melting regime (mode), a welding nozzle was used. For uniformity of the laser heating, the coordinate table with micrometric giving was used.

The x-ray method was used to determine the crystal lattice parameters, as well as to determine the amount of γ- and α-phases. The accuracy of determining the amount of martensite was 3–5%, the accuracy of measuring the lattice parameters — 10^{-4} nm. X-ray studies were performed on a DRON-3 diffractometer using a graphite monochromator in iron and cobalt radiation.

Residual stress measurements were performed by non-destructive x-ray method "$\sin^2\psi$". The method is based on the measurement of the elastic deformation of the crystal lattice [20]

$$\varepsilon = (d - d_0)/d, \tag{1}$$

where ε is an elastic deformation; d_0, d are the interplanar distances for unstrained and deformed lattices, respectively.

The residual stresses relate to the elastic deformation through the Hooke's law

$$\varepsilon = -\sigma\mu/E, \tag{2}$$

where E is a modulus of normal elasticity, and μ is the Poisson's coefficient.

To determine σ, it is required two measurements of deformation: one of them in the direction ψ normal to the surface — ε_ψ, and the second one — at an angle of ψ_0 to the surface of the sample — ε_0. The stresses are calculated as [20]

$$\sigma = \frac{E}{(1+\mu)} \frac{\varepsilon_\psi - \varepsilon_0}{\sin^2\psi - \sin^2\psi_0}, \tag{3}$$

The accuracy of stress measurement can be significantly improved by measuring the deformation for several values and making a linear graphical dependence of the interplanar distance $d = f(\sin^2\psi)$ using the least squares method. From the obtained graph, the values of d_1 and d_2 and the corresponding angles of inclination ψ_1 and ψ_2 are determined. In Ref. [20], the expression for calculating the stress value is obtained:

$$\sigma = \frac{E}{(1+\mu)} \frac{1}{d_0} \frac{d_2 - d_1}{\sin^2\psi_2 - \sin^2\psi_1}. \tag{4}$$

To eliminate the need to measure the unstressed sample, practically take d_0, equal to the value in the direction normal to the surface. The error from such replacement does not exceed 0.1%.

For practical use, it is convenient to translate this formula to the value of angles 2. To do this, we differentiate the Wolf–Bragg equation. Then, at λ = const, we obtain:

$$2d\cos\Theta \cdot \Delta\Theta + 2\Delta d \sin\Theta = 0, \tag{5}$$

from which

$$\Delta d/d = -\Delta\Theta \operatorname{ctg}\Theta \tag{6}$$

or

$$(d_2 - d_1)/d_0 = -\operatorname{ctg}\Theta_{\psi_1}(\Theta_{\psi_2} - \Theta_{\psi_1}), \tag{7}$$

where Θ_ψ is the value of the angle Θ that corresponds to the incline ψ. Taking into account Eqs. (5)–(7), we can write (4) as

$$\sigma = \frac{E}{1+\mu} \operatorname{ctg}\Theta_{\psi 1} \frac{\Theta_{\psi 1} - \Theta_{\psi 2}}{\sin^2\psi_2 - \sin^2\psi_1}, \tag{8}$$

Correlation $(\Theta_1 - \Theta_2)/(\sin^2\psi_2 - \sin^2\psi_1)$ is the coefficient, which characterizes the angle of inclination of the curve of $d = f(\sin^2\psi)$ to the abscissa, and accordingly the sign and nature of internal stresses.

Measurements were performed on the reflexes of each phase component, with sequential rotation of the sample at angles of 10°, 15°, 20°, 25°, and 30°, counting from the normal position.

A differential magnetometer assembled based on the BU-3 unit was used to measure the critical temperature points of the direct and reverse MT. The principle of magnetometer operation is a different orientation in the magnetic field of samples with paramagnetic (γ-phase) and ferromagnetic (α-phase) properties. The magnetometer consists of a powerful electromagnet, which provided the saturation field of 6000–7000 Oe. Between the poles of the electromagnet was a movable holder with fixed in it at an angle (70-80)° etalon (armco-iron) and investigated samples. Depending on the ratio of γ- and α-phases, the samples orient the holder in a magnetic field with an intermediate angle between the values, which it occupies in the case of using fully austenitic and fully ferritic samples. A mirror illuminated by a laser beam was fixed on the axis of the handle. The values of the angles were measured via the reflected beam on a pre-graduated linear scale. The accuracy of measuring the amount of martensitic phase was 0.3%.

The microstructure was analysed on a transmission electron microscope JEM-200CX and optical microscopes MIM-7, NeoPhot at a magnification from 100 to 1400. The grain size was determined with an accuracy of 0.1 μm. The microstructure of Fe–Ni alloys was detected by electrolytic etching in an electrolyte of (glycerol — 10%, perchloric acid — 20%, ethyl alcohol — 70%) at a voltage of 3 V. For better wetting of the samples, a small amount of surfactant was added in etchants. Various detergents were used as such substance. The etching time was selected experimentally depending on the contrast of the structure.

Metallographic investigations of the free and contact surfaces of the ribbons were made at low magnification without prior mechanical refining and etching, the same investigations at high magnifications after refining and etching, as well as oblique, longitudinal and transverse sections etched in a similar mode. In order to investigate the microstructure of the cross section the 4–7 glued ribbons of 2–3 cm long were filled with epoxy resin, after which they were ground with a fine abrasive and polished using chromium oxide powder. Electrolytic etching of such samples was performed in a solution of perchloric acid in the mode: voltage — 10 V, holding time — 10 s.

The distribution of Ni on the surface of the ribbon was determined on a scanning electron microscope JM6490LV using an x-ray spectral probe with a diameter of 1 μm and a penetration depth of 1 μm.

Measurement of the microhardness of the ribbon obtained by quenching from the melt was performed on the device PMT-3. A diamond pyramid with an angle between the faces of 136° was used as an indenter. Microhardness measurements were performed under an indenter load

from 25 g to 65 g. To obtain the correct results in different series of measurements, the load time (5 s) and exposure time under load (10 s) were permanent. The calculations of the microhardness HV and the depth of the imprint h were performed according to the following formulas:

$$HV = \frac{2ps\sin(\alpha/2)}{c^2}, \quad h = \frac{c}{2\mathrm{ctg}(\alpha/2)}; \tag{9}$$

here, p is the load on indenter, c is the length of the diagonal of the imprint, and a is the angle at the top of the indenter pyramid.

When measuring the microhardness of thin ribbons and surface layers, there is a limitation, which is that the depth of penetration of the diamond pyramid should be no more than 0.1 of the thickness of tested sample. For this reason, before measuring of the microhardness, the value of the critical penetration depth of the diamond pyramid was calculated (this was calculated for the smallest value of the ribbon thickness). Since the data on measuring the thickness of the ribbon indicated its significant heterogeneity, when measuring the microhardness of RQAs, the calculations were performed to measure the penetration depth of the diamond pyramid and in the case of penetration of the indenter to a depth more critical, the obtained microhardness value was considered incorrect.

3. Austenitic Phase Local Grain Structure of RQAs

Metallographic studies revealed significant heterogeneity of the macro- and microstructure of the ribbon [21–23]. The alloy *1* ribbon was characterized on both sides by roughness, the difference in the structure of the side sections (periphery) of the ribbon from its central part, the presence of gas cavities (GC) on the contact side and the presence of inflows and grooves on the free surface. These features of the macrostructure were related to the technology of the spinning process and are dependent mainly on the speed of the surface of the cooling disk and its quality. As noted in Ref. [24], increasing the speed of rotation of the disk led to a significant increase in the puddle of melt. This increased the area of actual contact of the ribbon with the disk, which in turn led to an increase in the heat transfer coefficient.

The free surface of the ribbon had a significant relief and consisted mainly of protrusions and depressions. The formation of protrusions on the surface of the ribbon was associated with the emergence of GC, when the solidification of the liquid melt occurred without contact with the surface of the cooling disk. Quenching of the melt in the area of depressions occurred directly on the surface of the disk. On the contact side, the individual areas with lines inherited from the surface of the disk were observed. Such areas in [24] are considered as areas of actual

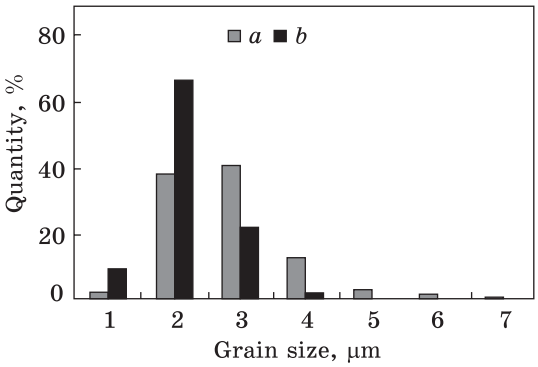

Fig. 1. Histogram of the distribution of average grain size in the area of the protrusion (*a*) and in the cavity (*b*) of the alloy *1* ribbon [21]

contact (AAC) of the melt with the disk. The area of AAC was approximately 30% of the total surface area of the ribbon. Confirmation of the fact of contact of the melt with the surface of the disk were the expressed lines and other features on the surface of the ribbon, which repeated the characteristic details of the relief of the imperfect surface of the disk. Features of the microstructure of AAC were transmitted through the entire cross section of the ribbon and therefore manifested both on the contact and on the free surfaces.

Areas of macrostructure with rounded inclusions were observed on the free surface. There were cavities around the inclusions. The inclusions were located within a non-AAC surface. The size of such inclusions averaged from 39 to 72 μm.

The internal structure of the "inclusions" can be determined by analysing the results of metallographic studies of the structure of ribbon after electrolytic etching. When focusing directly on the inclusion revealed the following features. The relief of the part of surface where the inclusions are located was very uneven and was as humps and cavities. The inhomogeneity of the grain structure can be traced on the oblique section of the ribbon, where differences in grain size and shape in local areas could be the result of the formation of humps and cavities on the free surface.

Based on the results of the analysis of images of the ribbon sections on the ledge and in the cavity, a histogram of the size distribution of austenitic grains was made [21] (Fig. 1).

The size of the original grain of austenite in the alloy *1* ribbons was mainly in the range 1.0–3.5 μm, and alloy *2* — in the range 0.5–2.0 μm. Ultrafine grains in the area of the protrusion were not observed under an optical microscope.

The above analysis applies to grains larger than 0.5 μm. Smaller grains were not detected in the optical microscope due to the physical limitation associated with the wavelength of the optical range. Apparently, a certain proportion of ultrafine grains was formed in the zone

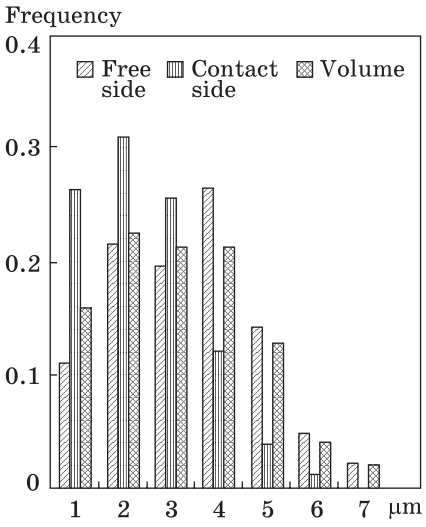

Fig. 2. The same as in the previous figure, but in the local areas [23]

close to the zone of contact of the jet with the surface of the disk.

Most grains had an equilibrium shape in all local areas of the ribbon. Averaging grain sizes (according to several dozen images, were measured the size of more than 500 grains for each local section of the ribbon) made it possible to build the histograms of the distribution of grains by size in the local areas of the ribbon [23] (Fig. 2). Image-Pro Plus (Media Cybernetics, Inc.) software was used to build the histogram of the grain size distribution.

As can be seen from Fig. 2, due to a significant difference in the cooling rate of the near-surface layers and the volume of the ribbon, the size of the equilibrium grains was differed significantly. For example, on the free side, the predominant amount (about 50%) are grains with a size of 3 to 5 μm, and on the contact side — 1–3 μm. Intermediate grains were observed in the volume (oblique section) of the ribbon. This different grain size distribution can be explained by different conditions and crystallization temperatures of the free contact side and the volume of the ribbon.

Due to the gradual heating of the disk surface in the ribbon material, relaxation processes developed, which resulted in almost complete absence of residual stresses in the ribbon, which were measured by the x-ray method $\sin^2\psi$. Internal stresses were absent at the beginning of the ribbon formation. This meant that during the solidification process there was a low-temperature (up to a quarter of melting temperature, $0.25T_m$), and as the disk heated — medium-temperature recrystallization (up to $(0.25–0.5)T_m$) [20].

On both surfaces and in a volume a certain number of three-grain joints with angles between the boundaries close to 120° were showed. Analysis of the evolution of triple intergrain joints during the formation of the ribbon allow to conclude about the development of recrystallization processes as a result of gradual heating of the cooler disk by liquid melt [23]. At the initial stage of ribbon formation (cold disk), the angles between the sides of the triple joints differed from 120° by 2–4°, and as the disk heated, this difference decreased, and at the end of the ribbon (warm disk) the angles differed by no more than two degrees. In parallel with this process, the number of triple joints increased, as well as the number of adjacent such joints increased. The successive manifes-

tation of these stages of formation of the grain structure, which contained triple joints of grains, testified to the gradual development of the recrystallization process during the formation of the ribbon due to the heating of the disk.

Electron microscopic studies of the alloys *1* and alloy *2* ribbons provided additional information regarding their microstructure [22, 23]. The size of the austenitic grain of the alloy *2* was 0.5–2 μm. The developed cellular structure with the sizes of cells 0.15–0.5 μm was observed in the grains. The initial grain size of the austenite of ribbon was larger and its magnitude was 1–3.5 μm. These data confirm the results of studies obtained by optical microscopy.

The density of dislocations in martensitic crystals was in the range of 10^{12} cm^{-2}. Austenite grains with a diameter of more than 1 μm in the vast majority were transformed almost completely into martensite. In grains with a diameter of less than 1 μm, MT was inhibited, and the amount of residual austenite increased with decreasing of a grain size.

The size and number of martensitic crystals decreased monotonically with decreasing of grain size. A noticeable decrease in the completeness of the transformation was observed already on grains with a diameter less than 1 μm. In grains with a diameter of 0.7 μm and less, the MT under conditions of deep cooling to the temperature of liquid nitrogen was not realized. Needle morphology of martensite in the studied range of austenitic grain sizes 0.8–4 μm did not change.

In Ref. [25], to explain the size effect of MT in thin ribbons of Fe–Ni alloys obtained by melt quenching, it was used the concept of the critical average size of austenitic grain, in which the γ–α-transformation was completely inhibited. Our experiments did not confirm this; in almost all grains below a certain size (0.6–0.7 μm), the transformation did not occur. The general regularity was that the completeness of the MT decreased with decreasing of austenitic grain size. As noted in Ref. [25], MT was observed in smaller grains, and larger grains were not transformed. This contradiction can be explained if we take into account that the structural state (density of dislocations, the presence of fragments with small angular subboundaries, internal stresses) differed significantly for different grains, especially in the range of sizes that are close to critical. Just the structural state of austenitic grains, favourable for the growth of the nucleus of the martensitic phase, could determine the experimental fact of the MT in smaller grains. The authors of Ref. [26] also previously concluded that the concept of critical average austenitic grain size, introduced in Ref. [25], is devoid of physical interpretation.

One of the manifestations of the heterogeneity of the ribbon's macrostructure was the formation of a specific mesh of perforation during the ribbons were rolled in rolls. At the first stage of rolling austenitic

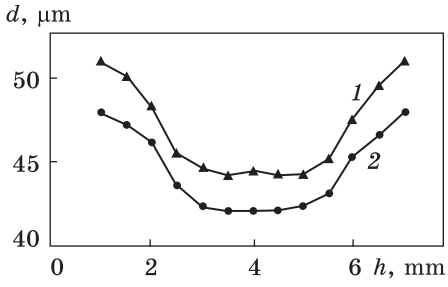

Fig. 3. The thickness, *d*, *vs*. the width, *h*, of alloy *1* ribbon, where *1* and *2* denote the cold and warm cooling disk, respectively [27]

grains are seen right along the rolling without breaking down the ribbon. At a farther, around the great grains, it was observed two regions of perforations. In a case of more equilibrium grains, a larger number of breaks were observed. At any grain size configuration, perforation always occurred along the grain boundaries. The formation of cracks was observed in the vast majority of cases in places of hollows, where the heterogeneity of the microstructure accumulated. The ribbon was torn in the weakest places (hollows, cavities).

When large grains were deformed, cracks and holes were formed mainly in one rolling direction, and when smaller grains were deformed, holes were formed chaotically. Analysis of the nature of microstructure of the areas where cracks occurred showed that in the process of rolling the ribbon with a thickness of 40 μm to a thickness of 20–15 μm cracks mainly occurred on the borders of the GH and ZFC. Subsequently, at a thickness of 12–5 μm, the cracks were elongated in the rolling direction, and the perforated ribbon took the form of a grid. The formation of such grid became possible under the condition of significantly different plasticity of the local sections of the ribbon. It should be noted that, in the process of rolling the ribbon to a thickness of 3–5 μm, it remained in the austenitic state.

Microstructural studies indicated the fact of significant heterogeneity and relief of the free and contact side. In this regard, the thickness of the ribbon was measured in width and length. The thickness was averaged by the results of 10–20 measurements lengthwise the line along the ribbon.

Measurement with a mechanical thickness gauge (accuracy — 1 μm) showed that the ribbon is inhomogeneous in thickness [27]. The difference in thickness at the edges and in the middle of the ribbon reached 8–10 μm (edge effect). This difference was observed along the entire length of the ribbon. The values of the thickness of ribbon at its end were smaller by 2–3 μm compared to the beginning. Such changes in thickness can be explained by the peculiarities of spraying and spreading of the jet on the disk with different temperatures. The graph of the change in thickness of the rapidly hardened ribbon of alloy *1* is presented in Fig. 3.

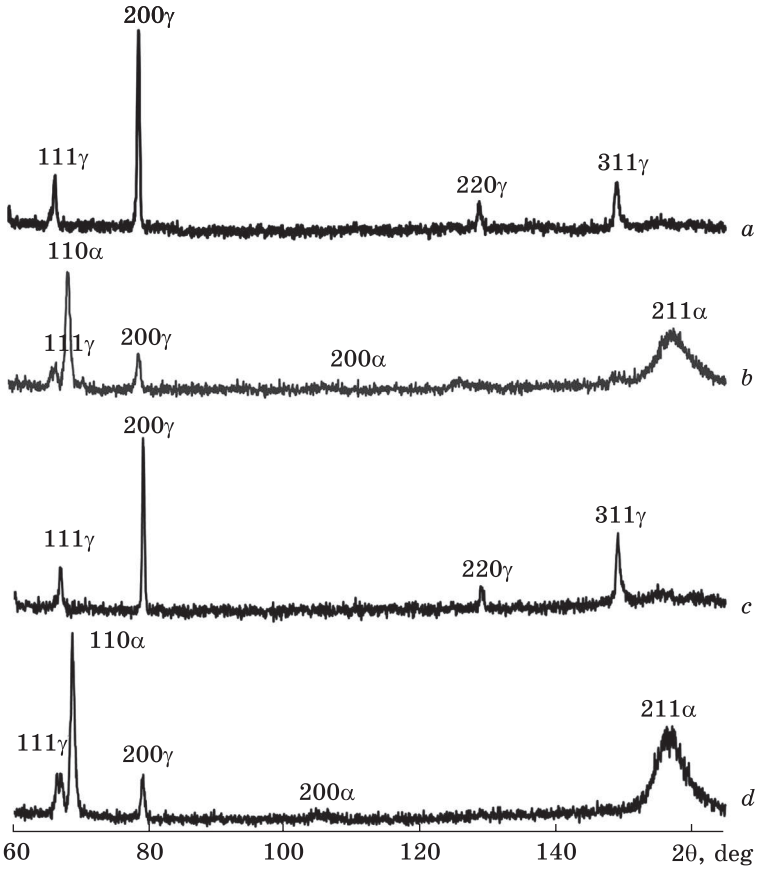

Fig. 4. ESR X-ray diffraction data (CrK_α radiation) of the alloy *1* ribbon free surface for the beginning (*a*, *c*) and end (*b*, *d*) of the ribbon in the austenitic (*a*, *b*) and two-phase α+γ (*b*, *d*) states [21]

The edge effect and the significant difference in thickness of the ribbon across the width, apparently, were the result of splashing the flow of melt on the surface of the disk, similar to the release of liquid from the centre of the drop that fell on a hard surface. This factor was more pronounced at the end of the period of ribbon formation, when the disk cooler was noticeably heated [28].

The inhomogeneous size distribution of austenitic grains in the local regions of the ribbons was appeared in the value of microhardness. In the study of the microhardness of alloy *1* ribbon, it was observed a significant discrepancy of its values for different regions of the ribbon. When measured at the beginning of the ribbon in the initial γ-state, it was found that the average value of microhardness on the contact side is 126 kg/mm^2, and on the free side of the ribbon — 98 kg/mm^2. The

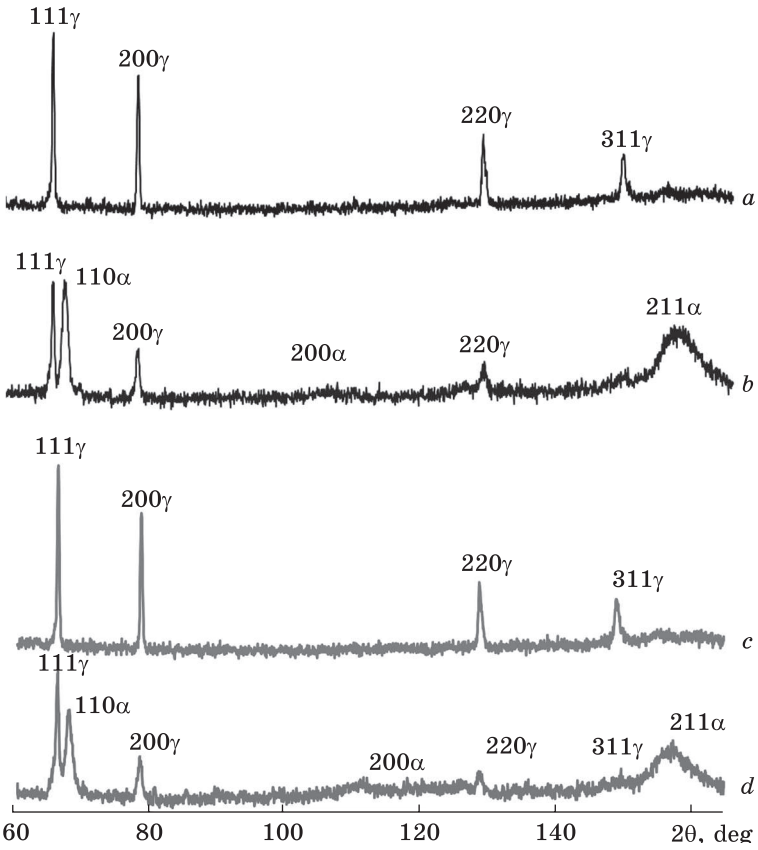

Fig. 5. The same as in the previous figure, but for the contact surface [21]

reason for the different microhardness on the free and contact side of the ribbon is due to the different grain size on them. On the contact side, the grain size was smaller than on the free side, so the microhardness of the fine-grained structure was higher.

When measuring the microhardness, depending on the width of the ribbon, an edge effect was observed: on the periphery of the ribbon, the microhardness was higher compared to its central part by 50–60 kg/mm^2 for the contact surface and 20–25 kg/mm^2 for the free surface. This difference was much smaller for both sides at the end of the ribbon (up to 10 kg/mm^2). Deviations of the value of microhardness from the average value clearly corresponded to the change in the value of austenitic grains.

Analysis of diffraction patterns from different local regions of the alloy *1* ribbon showed high texturing of the austenite structure on the free surface (Fig. 4). On the contact surface (Fig. 5), the ratio of the

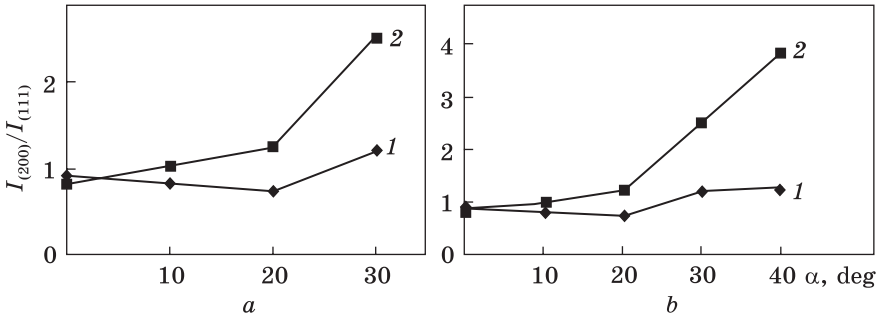

Fig. 6. The relative intensity $I_{(200)}/I_{(111)}$ of austenitic reflexes on the contact (*a*) and free (*b*) surfaces of the alloy *1* ribbon in the γ-state (beginning of the ribbon) *vs*. the angle α of the sample inclination to the Bragg position: *1* — $I_{(200)}/I_{(111)}$; *2* — $I_{(220)}/I_{(111)}$ [21]

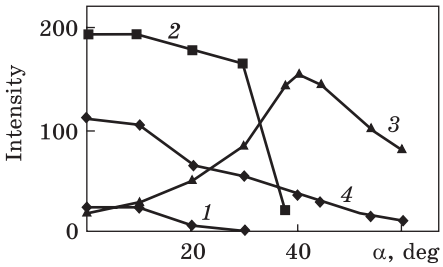

Fig. 7. The integral intensity for the free side of the alloy *1* ribbon (beginning of the ribbon) *vs*. the angle of inclination, α, relative to the Bragg position (for each reflex): *1* — $(111)_K$ ($2\Theta = 33.97°$); *2* — $(200)_K$ ($2\Theta = 39.95°$); *3* — $(220)_K$ ($2\Theta = 64.98°$); *4* — $(311)_K$ ($2\Theta = 74.95°$) [27]

intensity of austenitic reflexes I_{200}/I_{111} along the ribbon varied from 0.8 to 0.7, and for the free surface — from 4.5 to 5.8.

The austenitic phase on the free surface of the ribbon was formed with a growth texture of $(100)_\gamma$, characteristic of the f.c.c. structure. On the contact surface, this texture was much less pronounced. The degree of texturing markedly varied in width and length of the ribbon in accordance with the change in cooling rate during the crystallization of the ribbon. This difference in texture characteristics was determined by the higher cooling rate on the free surface and on the periphery of the ribbon.

The difference in texture on different sides of the ribbon was determined by the different cooling rate during its formation. The change in the nature of the texture along the length of the ribbon was associated with the beginning of the recrystallization process as we approached the end of the ribbon. The number of crystallites oriented in the plane (100) increased in the direction of the end of the ribbon on the free surface. The texture of austenite caused the texture of the next MT — the ratio of the intensity of martensitic reflexes differed significantly in the local areas of the ribbon (Figs. 4, *b*, *d* and 5, *b*, *d*). This difference in texture characteristics was determined by the higher cooling rate on the contact surface and on the periphery of the ribbon.

The presence of a texture of varying degrees on the contact and free surfaces can lead to a gradual change in the volume of the ribbon (internal texture). To test this assumption, x-rays of the ribbon surface were performed at different inclinations of the x-ray beam. The change in the relative intensity of diffraction reflexes (Fig. 6) indicated a continuous change in the degree of texture along the depth of the ribbon. The intensity of each of the austenitic reflexes varied according to certain regularities (Fig. 7).

4. Martensite Transformation Characteristics of RQAs

As shown in the previous section, the structural state of the ribbons obtained from RQAs was sharply inhomogeneous and differed significantly in local regions. Accordingly, the completeness of the direct MT (amount of martensitic phase) in the local regions of the ribbon was determined mainly by the volume fraction of the initial austenite with an ultrafine or nanocrystalline structure in which the transformation was inhibited partially or completely.

In the austenitic state at room temperature, the alloy *2* was paramagnetic and the alloy *1* was ferromagnetic. This made it possible to compare the magnetization σ of austenite of the alloy *1* ribbon with the magnetization of austenite of a bulk sample of the same alloy. The value of σ for ribbon austenite at room temperature was much smaller (49 $A \cdot m^2/kg$) than the same value of the bulk sample (82 $A \cdot m^2/kg$).

During the cooling to the temperature of liquid nitrogen in the ribbon and in the bulk sample of the alloy *1*, a direct martensitic γ-α-transformation took place, as a result of which the magnetization of the bulk sample and the ribbon in the α-state increased to 168 $A \cdot m^2/kg$ and 112 $A \cdot m^2/kg$, respectively (Fig. 8). Magnetometric curves in Fig. 8 characterize the completeness of the direct and reverse transformation. The Curie temperature, found by the temperature dependence of the saturation magnetization, decreased from 195°C for a bulk alloy to 165 °C for a ribbon. According to the literature data, the Curie point for the bulk alloy *1* is 190 °C, and the curves of the corresponding dependences have the usual shape for such systems [29].

The temperature T_s for the output ribbon, compared with the bulk sample, shifted towards lower temperatures by 30 °C and was 65 °C. The temperatures of the beginning, T_b, and the end, T_e, of the reverse MT for the alloy *1* ribbon also shifted towards lower temperatures by 35 °C and amounted of 300 and 380 °C, respectively.

In the alloy *2* ribbon, similar changes in the characteristics of MT were observed in comparison with the bulk alloy: the temperature of T_s decreased by 30 °C, and the amount of martensitic phase decreased by 20%. The Curie point for the ribbon was 150 °C at a value for a bulk

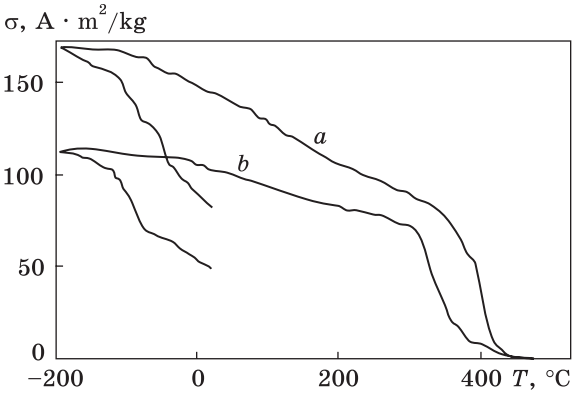

Fig. 8. Temperature (*T*) dependent magnetiza-tion (σ) of bulk alloy *1* (*a*) and alloy *1* ribbon (*b*) [29]

alloy of 305 °C. Similar to the alloy *1* ribbon, after the γ–α–γ-α transformation, the magnetization of the alloy *2* ribbon decreased by 48 A·m²/kg compared to the bulk sample.

Magnetometric measurements showed that in the ribbon took place a quite intense MT. These results were related to the average situation by the volume of the ribbon, because the different amounts of martensite were formed on the cross section and on different surfaces of ribbon. It is possible to measure more precisely the quantity of martensite in local areas of a ribbon only by an x-ray method. However, due to the significant texturing of the ribbon structure, the exact determination of the amount of martensitic phase by x-ray method was impossible.

Therefore, a method for determining the amount of martensitic phase in textured iron-based alloys has been proposed [30]. According to the proposed method, in contrast to other known methods, the integrated intensity of reflexes was measured only from those crystallographic planes of austenite and martensite that are parallel according to the crystallographic orientation relations between the crystal lattices of both phases. In the Fe-based alloys, different relations are realized:

$$\begin{gathered}(111)_\gamma \parallel (011)_\alpha, \\ [10\bar{1}]_\gamma \parallel [1\bar{1}1]_\alpha;\end{gathered} \tag{10}$$

$$\begin{gathered}(111)_\gamma \parallel (011)_\alpha, \\ [\bar{2}11]_\gamma \parallel [011]_\alpha;\end{gathered} \tag{11}$$

$$\begin{gathered}(111)_\gamma \parallel (011)_\alpha, \\ [\bar{5},12,17]_\gamma \parallel [7,\overline{17},17]_\alpha.\end{gathered} \tag{12}$$

The Kurdyumov–Sachs ratio (10) was obtained for the Fe–C system, and the Nishiyama (11) and Greninger–Troyano ratios (12) were obtained for Fe–Ni alloys with different nickel contents [1, 31]. For all types of relations, the same planes remain parallel, and the difference is only in parallel directions. This meant that the proposed method fully applies to alloys with different types of ratios.

For the martensitic γ–ε transformation, the planes $(111)_\gamma$ of austenite and $(0001)_\varepsilon$ of martensite are parallel:

$$\begin{aligned}(111)_\gamma \parallel (0001)_\varepsilon,\\ [10\bar{1}]_\gamma \parallel [2\bar{1}\bar{1}0]_\varepsilon.\end{aligned} \tag{13}$$

The idea of the method was to measure the intensity of x-ray diffraction reflexes from parallel planes of austenite and martensite, which does not change with different orientation (texture) of crystallites in the alloy due to the independence of the MT mechanism from the texture. The intensity of any other planes changes in accordance with the orientation (texture) of the crystallites, causing a significant decrease in the accuracy of the phase analysis (up to 30–50% or more). Compared with other methods, the proposed method is more accurate for textured alloys, since the amount of martensitic phase in different austenite crystallites does not depend on their orientation.

The method was carried out as follows. A flat sample of the alloy was mounted on a goniometer of the DRON-3 x-ray diffractometer, the sample was irradiated with a beam of characteristic x-rays, the diffraction pattern was recorded, and the integral intensity of diffraction x-ray reflexes for austenitic and martensitic phases was measured. Determination of the amount of martensitic phase was performed by the formula [32]:

$$M = \frac{I_{(hkl)_\alpha}}{P_\alpha} \frac{100}{I_{(hkl)_\alpha}/P_\alpha + I_{(hkl)_\gamma}/P_\gamma}, \tag{14}$$

where I is the integral intensity of diffraction x-ray reflexes of austenitic and martensitic planes, which are parallel, P_γ i P_α are the recurrence factors of these crystallographic planes of austenite and martensite.

This method was used to determine the amount of martensite for the ribbon of RQA *1* (Fig. 4) on the free surface of which the texture was observed. Another example of the texture under laser melting is shown in Fig. 9. For these cases, according to the orientation ratio, the planes $(111)_\gamma$ of austenite and $(011)_\alpha$ of martensite are parallel. Transforming formula (13) for this case, taking into account the relevant recurrence factors, we obtain the following formula:

$$M = \frac{I_{(011)_\alpha}}{12} \frac{100}{I_{(011)_\alpha}/12 + I_{(111)_A}/8}. \tag{15}$$

This method can also measure the amount of martensitic phase for the case of γ–ε transformation, *e.g.*, for iron–manganese textured alloy (Fig. 10). In this case, according to other orientation relations, the planes (111) and (0001) ε will be parallel. Taking into account the recurrence factors for these planes, we obtain the following formula:

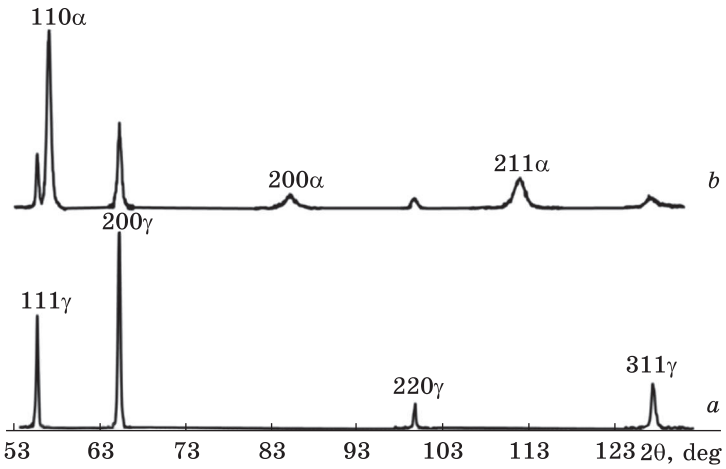

Fig. 9. X-ray diffraction pattern (FeK_α radiation) of a bulk alloy *2* after the laser melting (*a*) and subsequent cooling in the liquid nitrogen (*b*) [30]

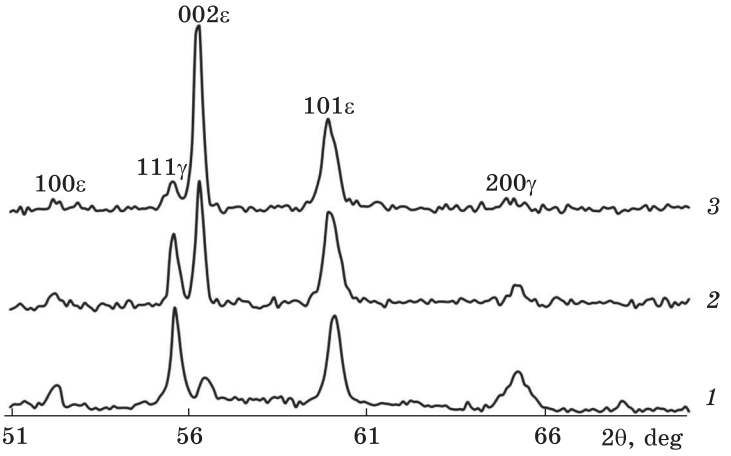

Fig. 10. X-ray diffraction pattern (FeK_α radiation) depending on the number of ε-cycles for a bulk Fe–18 wt.% Mn–2 wt.% Si alloy, where *1* — initial state, *2* and *3* — after one and ten ε-transformation cycles [30]

$$M = \frac{I_{(0001)_\varepsilon}}{2} \frac{100}{I_{(0001)_\varepsilon}/2 + I_{(111)_A}/8}. \qquad (16)$$

The problem of measuring the amount of martensite in the local regions of textured alloys has been also solved due to this method.

The proposed method for determining the amount of martensitic phase in metastable alloys with γ–α and γ–ε martensitic transformations can be

fully used to determine the number of other phases in materials with phase transformations of different types. For instance, with transformations of diffusion nature, for which the orientational relations between the initial and final crystal lattices are fulfilled: separation of carbide or nitride phases by decomposition of supersaturated solid carbon and nitrogen solutions, formation of oxides for oxidation of metals and alloys, *etc*.

Magnetometric and x-ray studies showed that the ribbons under cooling in liquid nitrogen was quite intense MT. Martensite with a bcc lattice with parameter of 0.2872 nm was formed in the alloy *1* ribbon. The martensite in the alloy *2* ribbon had a b.c.t structure with a tetragonality of 1.013. The tetragonality of carbon-free martensite of iron–nickel alloys was previously explained by coherent stresses between the martensite crystals and dispersed particles of the metastable γ′-phase of Ni_3Ti composition [33, 34].

Magnetometric curves gave the transformation parameters (characteristic temperature, amount of martensitic phase), averaged over the weight of the sample (0.5 g). X-ray phase analysis allowed estimating the amount of martensitic phase in the ribbon local areas (along the length and on different surfaces) regardless of the type of austenite texture. For this purpose, the experiments were performed on x-ray URS-0.02 equipment with a sharp focus and a beam diameter of 30 μm. X-ray study in a divergent beam with a difference of 2–3° gave the blurred diffraction lines. To increase the accuracy of measurements using samples in the cross-sections form, we used the method of diffraction lines focusing by G.V. Kurdyumov [2].

According to [32], for a certain Bragg angle, it is possible to select the angle of plane inclination to the primary x-ray beam, under which the conditions of focusing a given diffraction reflex are realized. In this way, it is necessary to register each reflex separately. As a result, various reflexes were registered, and the required accuracy of measurements in local areas of the cross-section was achieved. This position of the cross-section is determined by the formula from geometric considerations [31]:

$$\mathrm{tg}\alpha = \frac{\sin\Theta}{R/a + \cos\Theta}, \qquad (17)$$

where α is an angle formed by the plane of the cross-section and the direction of the primary x-ray beam, R is a radius of the chamber, and a is a distance of the cross-section from the first slit.

Thus, using a sharp-focus x-ray beam and focusing the x-ray reflexes according to G.V. Kurdyumov's method, we can perform diffraction measurements in local areas of flat samples.

The temperature T_s of the transformation beginning, measured by the magnetometric method, was lower by 40 °C as compared with the

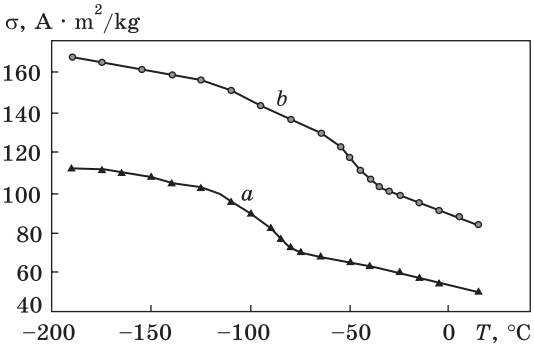

Fig. 11. The cooling temperature, *T*, dependent specific saturation magnetization, σ, for the ribbon (*a*) and bulk alloy *1* (*b*) [27, 35]

bulk alloy (Fig. 11). The completeness of the MT was different for different sides of the ribbon (Fig. 12, *a*, *b*). The 85% of martensite was formed on the free surface of alloy *1* and 57% on the contact surface (beginning of the ribbon). This does not correspond to the result of Ref. [10], where the amount of martensitic phase on the contact and free surfaces of the alloy *1* ribbon, rapidly quenched from the melt in an inert atmosphere, was equal to 93% and 60%, respectively. The different completeness of the transformation was explained in [10] by the nickel enrichment of the surface layer with a thickness of 10 μm from the free surface of the ribbon.

This difference in results can be filled with significantly different nickel redistribution processes when spinning a liquid jet in different atmospheres (carbon dioxide and inertial). It is obvious that for conditions of higher cooling rate in the atmosphere of carbon dioxide redistributed Ni practically did not occur.

The difference in the completeness of the MT on different surfaces of the ribbon was mainly determined by the grain size of the initial austenite. On the contact surface, the proportion of grains with ultrafine sizes was much larger. Inhibition of MT in such grains led to the fact that on the contact side the amount of martensitic phase was lower by 28% and 17% for alloys *1* and *2*, respectively.

As known, the completeness of the MT in iron–nickel alloys also depends on the chemical composition and the nature of the residual

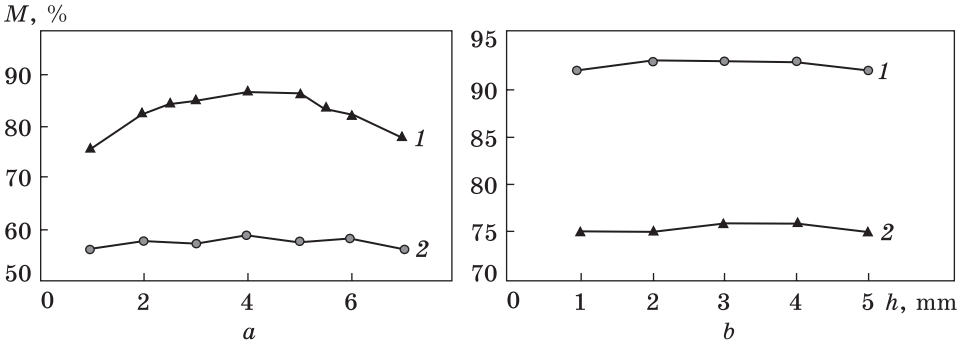

Fig. 12. The martensite volume fraction, *M*, *vs*. the width, *h*, of the ribbons of alloys *1* (*a*) and *2* (*b*) for the free (*1*) and contact (*2*) sides [36]

stresses. In this regard, the distribution of nickel in the ribbons was studied. It turned out that its content on the free surface of the ribbon was in 0.5–1.0 wt.% more than on the contact surface. The difference in the width of the ribbon was even smaller. Slight differences in nickel content could not explain the found difference in the volume fraction of martensite in different local areas of the ribbon.

The $\sin^2\psi$ calculations showed that a tensile residual stress of insignificant value (about 50 MPa) is formed on the contact side during crystallization, and there is practically no residual stress on the free surface. This stresses is also unable to affect significantly the fullness of MT.

Thus, the main factor of the changing of volume part of the martensite is the size effect at MT. The different completeness of the transformation in the local areas of the ribbon is mainly determined by the different volume fraction of ultrafine (0.5–1.0 μm) of the initial austenitic grains, in which the transformation was inhibited or supressed. Indeed, the analysis of the microstructure of the studied thin ribbons showed that the size of authentic grains that fell into the interval of action of the size effect in MT was determined.

The volume fraction of the martensitic phase and the characteristics of the martensitic transformations also varied continuously along the cross section of the ribbons. Thus, a double effect was observed for the alloy *1* ribbons: in addition to different amounts of martensitic phase on the free and contact side, in its central section on the free side the amount of martensitic phase was on 10–12% higher than in the nearside section (Fig. 19, *a*, curve *1*). On the contact side the edge effect was not observed (Fig. 12, *a*, curve *2*). For the alloy *2* ribbon, the edge effect was not expressed (Fig. 12, *b*, curve *1*). This was obviously due to the smaller width and possibly the thickness of this ribbon, which in turn resulted in a smaller difference in cooling rate across its width. Such changes in the characteristics of the structural-phase composition of the ribbon determined its gradient properties, which varied along its entire length.

The size effect at direct MT can effect on the carrying out of the reverse α–γ transformation in thin ribbons. In this regard, the effect of reverse α–γ transformation in microcrystalline ribbons on the completeness of the subsequent direct transformation and stabilization of reverted austenite was investigated.

The reverse transformation in the ribbons was carried out by slow heating at a rate of 0.08 deg/min an argon atmosphere to a temperature of 550 °C (alloy *1*) and 800 °C (alloy *2*). Under these conditions the γ-transformation had a diffusion character, which led to significant refining of reverted austenite grains due to the mechanism of multiple formation of γ-phase nuclei on various structural features of martensite, including on the boundaries of crystals, internal twins and excretions [33, 34].

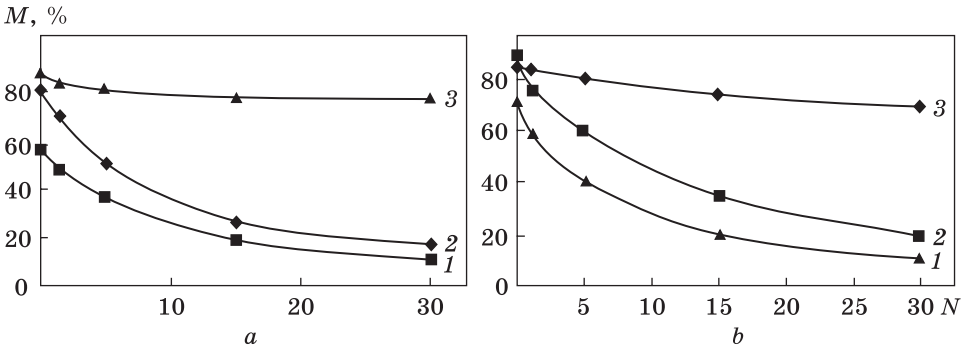

Fig. 13. The martensite volume fraction, M, *vs*. the quantity, N, of γ–α–γ transformations for contact (*1*) and free (*2*) sides of ribbon and for the bulk sample (*3*): *a* — alloy *1*; *b* — alloy *2* [44]

Because of this process, differently oriented nanosize lamellar crystals of reverted austenite with a thickness of 50–100 nm were formed [34–37]. For this reason, upon subsequent cooling in liquid nitrogen, the transformation was completely suppressed in such grains. For comparison, we studied the regularities of MT in a bulk sample of alloy *1*, from the ingot of which was cut a sample for spinning. It turned out that after the first cycle of transformation, cooling in liquid nitrogen led to the formation of 26% martensite; after the second one — 8% martensite; and only after the third transformation, cycle the reverted austenite was completely stabilized. These results showed that the degree of refining of the austenite by reverse transformation in the ribbon material was much higher than in a bulk alloy of the same chemical composition.

The reverse transformation, which took place when the alloy is heated to the appropriate temperature range at a rate higher than critical for this alloy, is non-diffusion. For the condition of such character of the atomic rearrangement, the stabilization degree of reverted austenite by transformations was much lower than in the case of the diffusion mechanism of reverse transformation. This is because the non-diffusion α–γ transformation did not change the sizes of the initial austenitic grains. Grains only fragmented depending on the number of cycles. After dozens of cycles, disoriented fragments of reverted nanoscale-level austenite (nanofragments) were formed [38–40]. Low-angle sub-boundaries were a less effective barrier for martensitic crystals compared to high-angle grain boundaries, but under the conditions of accumulation of the fragment misorientation at the accumulation of cycles, the completeness of the direct transformation decreased. The reduction in the size of the austenitic grain led to a more significant stabilization of the reverted austenite after reverse transformation with no diffusion char-

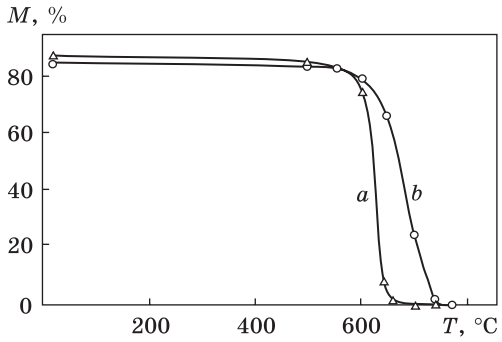

Fig. 14. The martensite volume fraction, M, *vs*. the heating temperature, T, for the reverse α–γ transformation in the quenched ribbon (*a*) and bulk (*b*) alloy *2* [44]

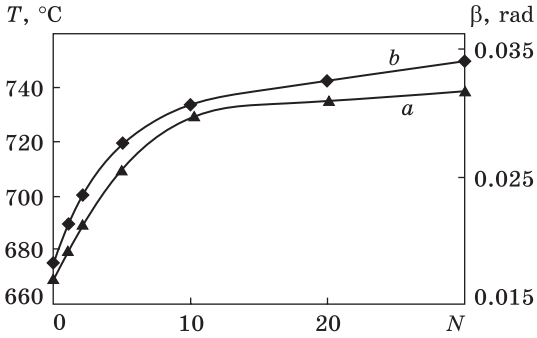

Fig. 15. The half-width, β, of the reflex $(311)_\gamma$ (*a*) and the final temperature of the α–γ transformation (*b*) *vs*. the number, N, of γ–α–γ transformations for the alloy *2* ribbon [40]

acter compared to the bulk sample of the same chemical composition. For the alloy *1* ribbon, it was found that after 30 cycles with non-diffusion α–γ transformation, the volume fraction of martensite on the free side of the ribbon decreased by 63% and on the contact side by 44%, while for the bulk sample this value decreased only by 8% (Fig. 13, *a*). A similar dependence was also found for the alloy *2* ribbon (Fig. 13, *b*).

The found regularity indicated that the size effect at the MT determined a higher degree of stabilization of reverted austenite by transformations on the free side of the ribbon (compared to the contact side).

In a comparative study of the effect of cycles' number on the characteristics of the structural-phase state of the ribbon and of the bulk alloy, it is necessary to take into account that the interval of α–γ transformation of the ribbon was shifted towards low temperatures. For the alloy *2* ribbon, according to x-ray data, this shift was approximately 80 °C (Fig. 14). Under conditions of increasing of the cycles number, the temperature T_k of the final transformations increased markedly (by 75–80 °C after 30 cycles, Fig. 15, curve *2*). At the same time, due to the accumulation of internal stresses in the process of thermal cycling, the half-width of the reflex (311) of the reverted austenite increased (Fig. 15, curve *1*). These results mean that to achieve a high degree of phase hardening from the transformations, it is necessary to heat the ribbon, quenched to martensite, under each subsequent transformation

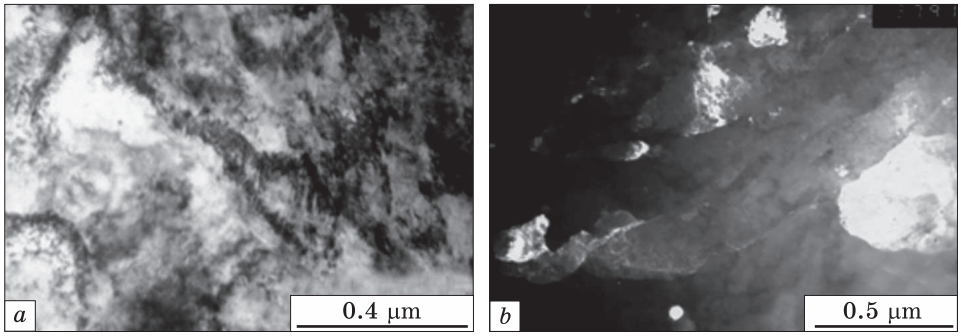

Fig. 16. The structure of the alloy *1* ribbon rolled to 5 μm (*a*), where *b* — the dark field image in the reflex $(111)_\gamma$ [23]

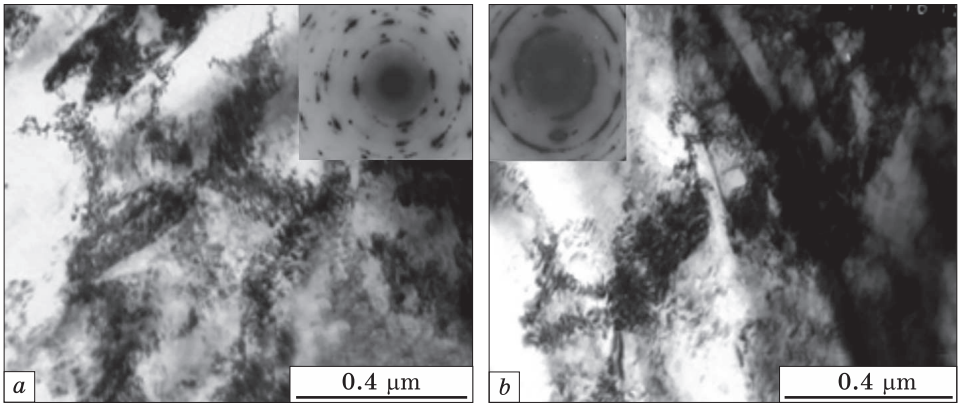

Fig. 17. The structure evolution of the alloy *2* ribbon rolled to a thickness of 8 (*a*) and 4 (*b*) μm [23]

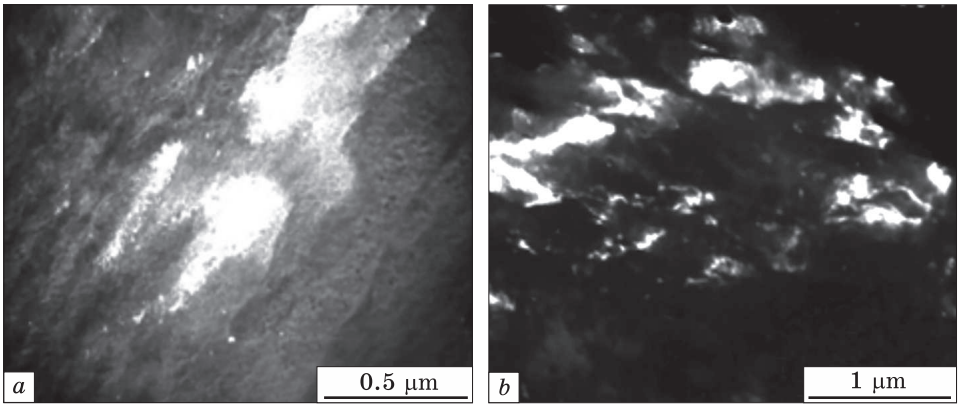

Fig. 18. Dark-field images in the reflex $(110)_\alpha$ from the structures shown in the previous figure [23]

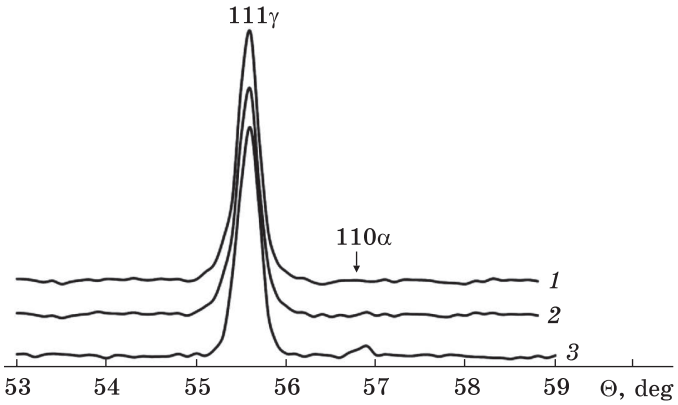

Fig. 19. Fragments of diffraction patterns (FeK_α radiation) from the alloy *1* ribbon, where *1* — initial state, *2* and *3* — after the rolling to a thickness of 5 and 1 μm, respectively [29]

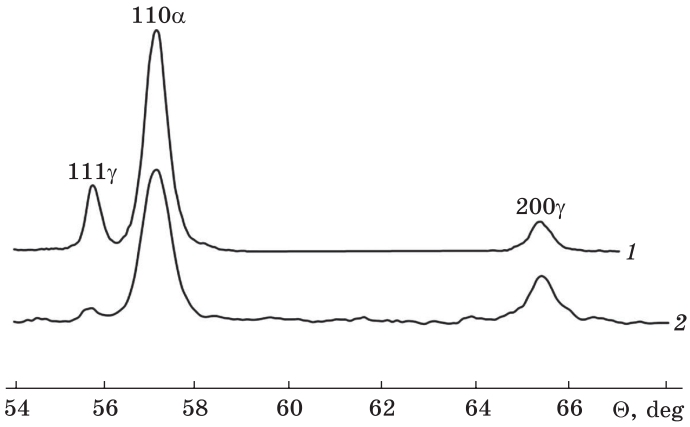

Fig. 20. Fragments of diffraction patterns (FeK_α radiation) from the alloy *1* ribbon after the cooling in liquid nitrogen (*1*), rolling to 5 μm followed with cooling in liquid nitrogen (*2*) [29]

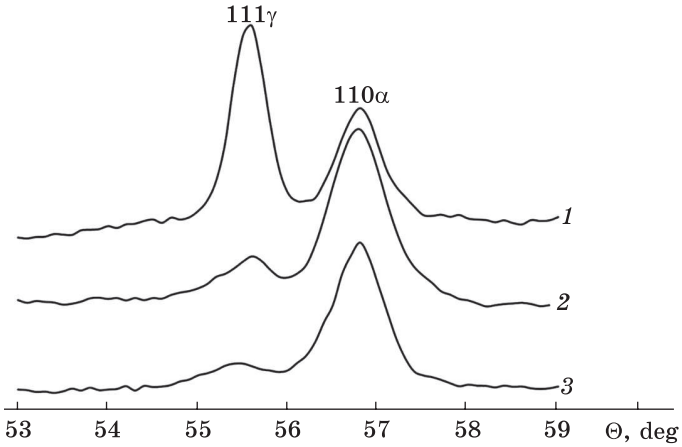

Fig. 21. Fragments of the diffraction pattern (FeK_α radiation) of alloy *2* ribbon, where *1* — contact side (initial state), *2* and *3* — after rolling to 5 and 1 μm, respectively [29]

to an ever-higher temperature T_k. This is due to the fact that overheating of the quenched alloy above the temperature T_k already at 10–15 °C leads to the development of relaxation processes and a corresponding decrease in the degree of phase hardening.

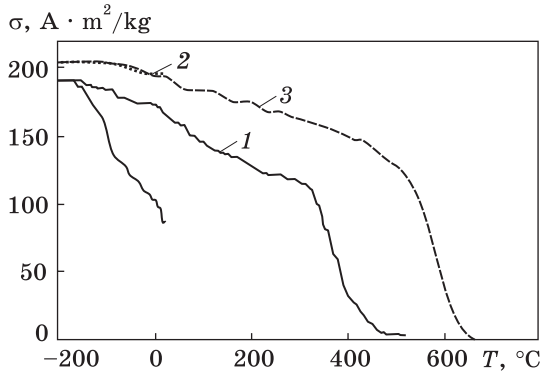

Fig. 22. Temperature dependent magnetization of the ribbons rolled to a thickness of 5 μm of alloy *1* (*a*) and alloy *2* (*b*, *c*): *a* — cooling in liquid nitrogen and heating to final temperature T_e, cooling in liquid nitrogen (*b*) with subsequent heating to T_e (*c*) [48]

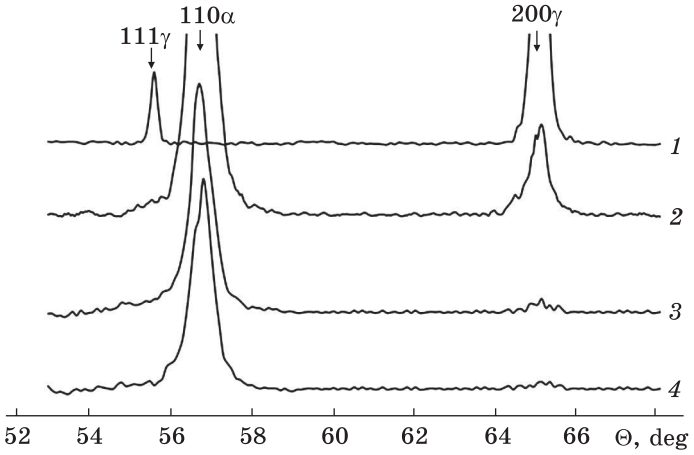

Fig. 23. Fragments of the diffraction pattern (FeK_α radiation) of the alloy *2* ribbon: *1* — free side (initial state), *2* — cooling in liquid nitrogen, *3* — rolling to a thickness of 5 μm, *4* — cooling of the rolled ribbon (up to 5 μm) in liquid nitrogen [48]

In the Fe-based alloys, the MT is sensitive to plastic deformation of initial austenite [41–43]. During the plastic deformation of austenite, it can both activate and inhibit subsequent MT [44–47]. In this regard, additional refining of the austenitic structure can be obtained by rolling of the ribbons.

Electron microscopic studies of the structure of rolled ribbons were performed (Figs. 16–18). The alloy *1* ribbon was sequentially rolled to a thickness of 10, 5, 3, and 1 μm; and the alloy *2* ribbon was rolled to a thickness of 6, 4, and 2 μm. Sequential rolling of the alloy *1* ribbon to 10 μm did not lead to deformation-induced MT. After rolling to 5 μm, the x-ray diffraction pattern contained reflexes of a small amount (7%) of the martensitic phase (Figs. 19–21, curve *1*). The electronic microdiffraction pattern also contained martensitic reflexes. A cellular submicrostructure with a size of fragments from 0.5 to 0.1 μm was formed in the deformed ribbon (Fig. 16).

The evolution of the ribbon structure with increasing degree of plastic deformation during the rolling is shown in Figs. 17 and 18. At the first stage of rolling a cellular substructure was formed. The size of

the fragments ranged from 0.5 to 0.1 μm. The walls of the cells were three-dimensional formations in the form of tangled dislocations with a density of about 10^{11} cm^{-2}. In the structure of the ribbon, rolled up to 2 μm, there were broken boundaries. As the degree of deformation increased, an increase in the angle of disorientation between the cells was observed. This was evidenced by the change in the form of electron microdiffraction from electron patterns with one axis of the zone and a slight azimuthal blurring of reflexes to almost circular electron patterns.

Rolling of the alloy *2* ribbon to 5 μm caused intensive development of MT (about 95% martensitic phase) (Fig. 21; Fig. 23). Cooling of the deformed ribbons in liquid nitrogen did not cause an additional MT. Microelectron patterns contained the reflexes from f.c.c. and b.c.c. phases (Fig. 17). After rolling to 6, 4, and 2 μm, the structure of the ribbon was transformed into single-phase with b.c.c. martensite (Figs. 17, *b* and 18, *b*).

Magnetometric studies confirmed that, because of cooling in liquid nitrogen of the ribbon rolled to a thickness of 3 μm, an intense MT happened (Fig. 22, curve *1*). The temperature T_s for the rolled ribbon is reduced by 15 °C compared to the initial ribbon. Cooling of the alloy *2* ribbon rolled to a thickness of 1 μm did not change the amount of martensite (Fig. 22, curve *2*). The next heating led to the reverse $\alpha-\gamma$ transformation in both ribbons (Fig. 22, curves *1* and *3*). The temperature of the T_s and T_e ribbons remained practically unchanged compared to the initial one, unstrained ribbons.

5. Conclusions

The grain structure of the austenitic phase in thin ribbons of iron-nickel alloys, rapidly quenched from the melt, was formed sharply inhomogeneous and differed not only on the contact and on free surfaces, but on the width and length of the ribbon too. Deviation of grain size distribution from homogeneous can be explained by different cooling rate in local areas of the ribbon. The ribbons were also heterogeneous in thickness. The difference in thickness at the edges and in the centre of the ribbon reached 8 μm, and at the end of the ribbon was smaller by 2–3 μm compared to the beginning. The decrease in the thickness of the ribbon was due to the decrease in the adhesion of the ribbon to the surface of the cooler disk when a liquid jet heated it.

The formation of the grain structure occurred with the gradual heating of the disk. The result was the practical absence of residual stresses in the austenitic phase, the formation of triple equilibrium grain boundaries and an increase in grain size up to several times, as we approached the end of the ribbon. This meant that the quenching effect along the ribbon was not permanent.

Due to the significant difference in the cooling rate on the free side, a pronounced one-sided axial texture of the growth of the austenitic phase was formed along the $(100)_\gamma$ plane, the degree of which varied along the width and length of the ribbon. On the contact side, the same texture of austenitic grains was weakly expressed.

The size of the original grain of austenite in the alloy *1* ribbons was mainly in the range of 1.0–3.5 μm, and alloy *2* — in the range of 0.5–2.0 μm. The grains had a developed cellular structure with cell sizes of 0.15–0.5 μm. After cooling the ribbons in liquid nitrogen, the martensitic crystals had needle morphology. In grains with a diameter of more than 1 μm, almost completely martensitic structure was observed. In grains with a diameter of 1.0–0.8 μm, the completeness of the MT decreased markedly, and in grains with a diameter of less than 0.7 μm, the transformation did not take place (edge effect).

The amount of martensite on the free side of the ribbon was increased by 17% in alloy *1* and 28% in alloy *2* as compared to the contact side. An edge effect was found on the width of the ribbon of alloy *1*: in the central part of the free side, the amount of martensite was greater by 10–12% than in the side (peripheral). There was not an edge effect observed on the contact side. The established regularities of the distribution of the amount of martensitic phase can be fully explained by the size distribution of austenitic grains, since these dimensions fell within the range of the size effect at MT. Significantly inhomogeneous size distribution of austenitic grains in local areas of the ribbon and a pronounced size effect in MT led to the formation of gradient properties of thin ribbons of RQAs.

Compared with bulk alloys, the size effect in MT determined a higher degree of stabilization of reversed austenite of thin ribbons by reverse α–γ transformations. The stabilization effect took place for both diffusion and non-diffusion character of α–γ transformation. The reverse α–γ transformation of diffusion character, realized in the ribbon at slow heating with a speed in α–γ-interval less than 0.5 deg/min, led to significant refining of the initial austenitic grain through the diffusion mechanism of multiple nucleation of γ-phase on the structure defects of martensitic phase. As a result, the reversed austenite after one α–γ transformation of diffusional character was completely stabilized in relation to the direct MT during subsequent cooling in liquid nitrogen. With the non-diffusion character of α–γ transformations (rapid heating in the α–γ interval), it is possible to repeat them many times without significant stabilization of the reversed austenite. In thin ribbons, the degree of phase hardening from the cycles of γ–α–γ transformations was achieved lower compared to bulk alloys of the same chemical composition.

REFERENCES

1. L.I. Lysak and B.I. Nikolin, *Phizicheskie Osnovy Termicheskoi Obrabotki Stali* [Physical Fundamentals of Thermal Treatment of Steel] (Kiev: Technika: 1975) (in Russian).
2. G.V. Kurdyumov, *Problems of Metal Science and Physics of Metals*, No. 3: 9 (1952) (in Russian).
3. A.L. Roitburd, On the thermodynamics of martensite nucleation, *Mater. Sci. Eng. A*, **127**, No. 2: 229 (1990); https://doi.org/10.1016/0921-5093(90)90313-R
4. V.A. Lobodyuk and E.I. Estrin, *Martensitic Transformations* (Cambridge International Science Publishing Ltd: 2014).
5. A. Inoue, Y. Kojima, T. Minemura, and T. Masumoto, Microstructure and mechanical properties of ductile Ni_3Al-type compound in Fe–(Ni, Mn)–Al–C systems rapidly quenched from melts, *Metallurgical Trans.*, **12**: 1245 (1981); https://doi.org/10.1007/BF02642338
6. O.V. Letenkov, *Formirovanie Structury i Funkcionalnykh Svoistv Tonkorazmernykh Lent iz Splavov na Osnove Medi, Poluchennykh Spiningovaniem Rasplava* [Structure Formation and Functional Properties of Thin-Sized Ribbons from Copper-Based Alloys Obtained by Melt Spinning] (Thesis of Disser. for Cand. Phys.-Math. Sci. — Ph.D.) (Novgorod: 2006) (in Russian).
7. S.G. Zaichenko and A.M. Glezer, Disclination mechanism of plastic deformation of nanocrystalline materials, *Interface Sci.*, **7**: 57 (1999); https://doi.org/10.1023/A:1008714612121
8. A.M. Glezer, E.N. Blinova, V.A. Pozdnyakov, and A.V. Shelaykov, Martensite transformation in nanoparticles and nanomaterials, *Journal of Nanoparticle Research*, **5**: 551 (2003); https://doi.org/10.1023/B:NANO.0000006094.08917.46
9. K. Yamauchi and Y. Yoshihito, Structure and mechanical properties of liquid-quenched nanocrystals, *Mater. Sci. Forum*, **225–227**: 781 (1996); https://doi.org/10.4028/www.scientific.net/MSF.225-227.781
10. E.N. Blinova, A.M. Glezer, V.A. Diakonova, and V.A. Zorin, *Izv. RAS. Physics*, **65**, No. 10: 1444 (2001) (in Russian).
11. V.Y. Bondar, V.E. Danilchenko, V.F. Mazanko, O.V. Filatov, and V.E. Iakovlev, Effect of cyclic martensitic γ–ϵ–γ transformations on diffusion characteristics of carbon in an iron–manganese alloy, *Prog. Phys. Met.*, **19**, No. 1: 70 (2018); https://doi.org/10.15407/ufm.19.01.070
12. V.Yu. Danilchenko, V.F. Mazanko, O.V. Filatov, and V.E. Iakovlev, Effect of cyclic martensitic γ–ϵ transformations on diffusion characteristics of cobalt in an iron–manganese alloy, *Prog. Phys. Met.*, **20**, No. 3: 426 (2019); https://doi.org/10.15407/ufm.20.03.426
13. V.A. Tatarenko, S.M. Bokoch, V.M. Nadutov, T.M. Radchenko, and Y.B. Park, Semi-empirical parameterization of interatomic interactions and kinetics of the atomic ordering in Ni–Fe–C permalloys and elinvars, *Defect Diffus. Forum*, **280–281**: 29 (2008); https://doi.org/10.4028/www.scientific.net/DDF.280-281.29
14. V.A. Tatarenko and T.M. Radchenko, The application of radiation diffuse scattering to the calculation of phase diagrams of f.c.c. substitutional alloys, *Intermetallics*, **11**, Nos. 11–12: 1319 (2003); https://doi.org/10.1016/S0966-9795(03)00174-2

15. T.M. Radchenko and V.A. Tatarenko, Atomic-ordering kinetics and diffusivities in Ni–Fe permalloy, *Defect Diffus. Forum*, **273–276**: 525 (2008); https://doi.org/10.4028/www.scientific.net/DDF.273-276.525
16. T.M. Radchenko, V.A. Tatarenko, and S.M. Bokoch, Diffusivities and kinetics of short-range and long-range orderings in Ni–Fe permalloys, *Metallofiz. Noveishie Tekhnol.*, **28**, No. 12: 1699 (2006).
17. T.M. Radchenko, O.S. Gatsenko, V.V. Lizunov, and V.A. Tatarenko, Martensitic α''-$Fe_{16}N_2$-type phase of non-stoichiometric composition: current status of research and microscopic statistical-thermodynamic model, *Prog. Phys. Met.*, **21**, No. 4: 580 (2020); https://doi.org/10.15407/ufm.21.04.580
18. T.M. Radchenko, V.A. Tatarenko, H. Zapolsky, and D. Blavette, Statistical-thermodynamic description of the order–disorder transformation of $D0_{19}$-type phase in Ti–Al alloy, *J. Alloys Compd.*, **452**, No. 1: 122 (2008); https://doi.org/10.1016/j.jallcom.2006.12.149
19. I.S. Miroshnichenko and I.V. Sally, *Zavodskaya Laboratoriya*, **25**, No. 11: 1398 (1959) (in Russian).
20. N.I. Komyak and U.G. Myasnikov, *Rentgenovskie Metody i Oborudovanie dlia Opredeleniya Napriazeniy* [X-Ray Methods and Equipment for the Stresses Determination] (Leningrad: Mashinostroenie: 1972) (in Russian).
21. V.Yu. Danil'chenko, E.M. Dzevin, R.M. Delidon, and V.K. Nosenko, *Metallofiz. Noveishie Tekhnol.*, **33**, No. 4: 535 (2011).
22. I.I. Kositsyna, V.V. Sagaradze, and V.E. Danil'chenko, Structure and properties of manganese austenitic steels quenched from the melt, *Phys. Metals Metallogr.*, **109**, No. 6: 643 (2010); https://doi.org/10.1134/S0031918X10060116
23. V.E. Danil'chenko, R.N. Delidon, I.I. Kositsina, and V.V. Saragadze, Martensitic transformation in an iron-nickel melt-quenched alloy, *Phys. Metals Metallogr.*, **111**: 253 (2011); https://doi.org/10.1134/S0031918X11020050
24. V.K. Nosenko, *Issledovanie Protsessov Formirovaniya Structury i Svoistv Splavov Fe–Si, Poluchennykh v Razlichnykh Usloviyakh Sverkhbystroi Zakalki iz Rasplava* [Investigation of the Processes of Structure Formation and Properties of Fe–Si Alloys Obtained in the Different Conditions of Super-Fast Quenching the Melt] (Thesis of Disser. for Cand. Phys.-Math. Sci. — Ph.D.) (Kiev: G.V. Kurdyumov Institute for Metal Physics of the N.A.S. of Ukraine: 1990) (in Russian).
25. A.M. Glezer, I.V. Maleeva, and N.G. Novoselova, Effect of quenching from melt on the structure and properties of Fe–Cr–Al alloys, *Fiz. Met. Metalloved.*, No. 1: 122 (1990) (in Russian).
26. V.A. Lobodyuk, A size effect at the martensitic transformation, *Fiz. Met. Metalloved.*, **99**, No. 2: 29 (2005) (in Russian).
27. V.J. Bondar, V.Yu. Danilchenko, R.M. Delidon and V.K. Nosenko, *Nanosistemi, Nanomateriali, Nanotehnologii*, **7**, No. 1: 305 (2009) (in Ukrainian); https://www.imp.kiev.ua/nanosys/media/pdf/2009/1/nano_vol7_iss1_p0305p0314_2009.pdf
28. V.K. Nosenko, *Formirovanie Amorfnyh i Nanokristallicheskikh Sostoianiy v Splavakh na Osnove Fe i Al* [Formation of Amorphous and Nanocrystalline States in the Fe- and Al-Based Alloys] (Thesis of Disser. for Dr. Phys.-Math. Sci.) (Kyiv: G.V. Kurdyumov Institute for Metal Physics of the N.A.S. of Ukraine: 2005) (in Russian).
29. V.E. Danilchenko and R.M. Delidon, *Physical and Chemical Bases of Formation and Modification of the Micro- and Nanostructures* (Kharkiv: 2011), **2**, p. 338 (in Ukrainian).

30. V.E. Danilchenko, V.J. Bondar, and Ie.M. Dzevin, *Sposib Termotsiklichnogo Obroblennia Stali z Obernenym Martensytnym Peretvorenniam* [Thermal–Cyclic Method of Treatment of the Steel with Reversed Martensitic Transformation], Authors Certificate 94485 Ukraine (Published November 10, 2014) (in Ukrainian).
31. G.V. Kurdyumov, L.M. Utevskiy, and R.I. Entin, *Prevrashcheniya v Zheleze i Stali* [Transformations in Iron and Steel] (Moskva: Nauka: 1977) (in Russian).
32. L.I. Mirkin, *Rentgenovskiy Analiz Polikristallov* [X-Ray Analysis of Polycrystals] (Moskva: 1961) (in Russian).
33. Yu.N. Koval and V.V. Kokorin, Tetragonality of the carbon-free martensite, *Fiz. Met. Metalloved.*, **39**, No. 5: 1044 (1975) (in Russian).
34. M.M. Hal, P.G. Winchell, and P. Guy, Tetragonality of Fe–Ni–Ti martensite, *Acta Met.*, **25**, No. 7: 735 (1977);
https://doi.org/10.1016/0001-6160(77)90089-X
35. V.E. Danilchenko and R.M. Delidon, *Z. Kristallogr. Proc.*, X-ray studies of martensitic transformation in Fe–Ni alloys rapidly quenched from the melt, **1**: 267 (2011);
https://doi.org/10.1524/9783486991321-045
36. V. Bondar, V. Danilchenko, and Ie. Dzevin, Gradient distribution of martensite phase in melt-spun ribbons of a Fe–Ni–Ti–Al alloy, *Nanoscale Res. Lett.*, **11**: 96 (2016);
https://doi.org/10.1186/s11671-016-1313-0
37. E.P. Pechkovskiy and V.I. Trefilov, *Ukr. J. Phys.*, No. 16: 133 (1971) (in Russian).
38. P.U. Volosevich, V.N. Gridnev, and Yu.N. Petrov, *Metallofizika*, No. 57: 28 (1975) (in Russian).
39. P.U. Volosevich and Yu.N. Petrov, *Metallofizika*, No. 1: 20 (1975) (in Russian).
40. K.A. Malyshev, V.V. Sagaradze, I.P. Sorokin, A.I. Uvarov, V.A. Teplov, and N.D. Zemtsova, *Fazovyy Naklep Austenitnykh Splavov na Fe–Ni Osnove* [Phase Cold Work Hardening of Fe–Ni-Based Austenite Alloys] (Moskva: Nauka: 1982) (in Russian).
41. G.J. Thomas, R.W. Siegel, and J.A. Eastman, Grain boundaries in nanophase palladium: high resolution electron microscopy and image simulation, *Scripta Metal. Mater.*, **24**, No. 1: 201 (1990);
https://doi.org/10.1016/0956-716X(90)90592-5
42. S. Ranganathan, R. Divakar, and V.S. Raghunathan, Interface structures in nanocrystalline materials, *Scripta Mater.*, **44**, Nos. 8–9: 1169 (2001);
https://doi.org/10.1016/S1359-6462(01)00678-9
43. V.G. Gorbach, E.A. Izmailov, and I.S. Panpanza, Electron microscopic study of the transformation of martensite into austenite, *Fiz. Met. Metalloved.*, **34**, No. 6: 1238 (1972) (in Russian).
44. V.I. Bondar, V.Ie. Danilchenko, and Ie.M. Dzevin, Structure fragmentation in Fe-based alloys by means of cyclic martensitic transformations of different types, *Nanoscale Res. Lett.*, **9**: 92 (2014);
https://doi.org/10.1186/1556-276X-9-92
45. V.V. Rybin, *Bolshie Plasticheskie Deformatsii i Razrushenie Metallov* [Big Plastic Deformations and Fracture of Metals] (Moskva: Metallurgiya: 1986) (in Russian).
46. I.I. Kositsina, S.V. Kositsin, and V.V. Sagaradze, *Metal Science and Heat Treatment*, No. 6: 21 (1992) (in Russian).
47. V.I. Arkharov, Kristallografiya Zakalennoy Stali [Crystallography of Hardened Steel] (Moskva: Metallurgiya: 1951) (in Russian).

48. V. Danilchenko, Ie. Dzevin, and V. Sagaradze, Effect of multiple martensitic transformations on structure of Fe–Ni alloys, *J. Mater. Sci. Technol.*, **29**, No. 3: 279 (2013);
https://doi.org/10.1016/j.jmst.2012.12.016

Received 13.05.2021;
in final version, 31.01.2022

В.Ю. Данільченко, Є.М. Дзевін, Р.М. Делідон
Інститут металофізики ім. Г.В. Курдюмова НАН України,
бульв. Академіка Вернадського, 36,
03142 Київ, Україна

ЗАКОНОМІРНОСТІ МАРТЕНСИТНИХ ПЕРЕТВОРЕНЬ
Fe–Ni-СТОПІВ, ШВИДКОЗАГАРТОВАНИХ ІЗ РОЗТОПУ

Оглянуто та досліджено закономірності формування зеренної структури метастабільних залізоніклевих стопів, сформованої в умовах високих температурних ґрадієнтів за гартування із розтопу (спінінґування), та її вплив на характеристики мартенситних перетворень (МП) у локальних областях тонких стрічок. Проведено порівняння текстури аустенітної та мартенситної фаз на різних сторонах тонких стрічок. Досліджено наслідки впливу релаксаційних процесів упродовж твердіння тонких стрічок на закономірності формування зеренної структури. Запропонований рентґенівський спосіб міряння кількости мартенситу уможливив вирішення задачі вимірювання кількости мартенситу в локальних областях текстурованих стопів. Встановлено, що повнота МП є різною для контактної та вільної сторін стрічки. Проаналізовано основні чинники, які визначили неоднорідний розподіл мартенситної фази в локальних областях стрічки. Проаналізовано вплив розмірних ефектів за МП, залишкових напружень і зміни хемічного складу аустенітної фази на розподіл мартенситної фази в локальних ділянках стрічки. Досліджено вплив розмірного ефекту на перебіг прямого γ–α- і зворотнього α–γ-МП у тонких стрічках. Виявлено роль ультрадисперсної складової аустенітних зерен у стабілізації аустеніту швидкозагартованих стопів циклічними γ–α–γ-МП.

Ключові слова: мартенситні перетворення, стопи Fe–Ni, спінінґування розтопу, стрічка, зеренна структура, текстура, напруження.